

Article

Condensation Risk Due to Variations in Airtightness and Thermal Insulation of an Office Building in Warm and Wet Climate

Wanghee Cho ^{1,*}, Shizuo Iwamoto ² and Shinsuke Kato ¹

¹ Institute of Industrial Science, The University of Tokyo, 4-6-1 Komaba, Meguro-ku, Tokyo 153-8505, Japan; kato@iis.u-tokyo.ac.jp

² Department of Architecture, Faculty of Engineering, Kanagawa University, 3-27-1 Rokkakubashi, Kanagawa-ku, Yokohama 221-8686, Japan; iwamos01@kanagawa-u.ac.jp

* Correspondence: chowh@iis.u-tokyo.ac.jp; Tel.: +81-3-5452-6430; Fax: +81-3-5452-6432

Academic Editor: Hossam A. Gabbar

Received: 5 August 2016; Accepted: 19 October 2016; Published: 27 October 2016

Abstract: Condensation in a building encourages microbial growth, which can have an adverse effect on the health of occupants. Furthermore, it induces the deterioration of the building. To prevent problems caused by condensation, from the design step of a building, predictions of the spatial, temporal and causation for condensation occurrences are necessary. By using TRNSYS simulation coupled with TRNFLOW, condensation assessment of an entire office building in Tokyo, Japan, was conducted throughout the year, including when the air-conditioning system was not operated, by considering the absorption-desorption properties of the building materials and papers in the office and the airflow within the entire building. It was found that most of the condensation occurred during winter and was observed mainly in the non-air-conditioned core parts, especially the topmost floor. Additional analyses, which identified the effect of variations in the thermal insulation of the external walls, roof and windows and the airtightness of the windows on condensation, showed that the lower airtightness of windows resulted in decreased condensation risks, and condensation within the building was suppressed completely when the thermal insulation material thickness of the external walls was greater than 75 mm, that of the roof was greater than 105 mm and the windows had triple float glass.

Keywords: condensation risk (CR); microbial growth; airtightness; thermal insulation; office building; warm and wet climate

1. Introduction

Moisture in a building directly affects an occupant's thermal comfort and health and induces corrosion of the building. Furthermore, moisture is an essential factor for designing an air-conditioning system. Therefore, it is necessary to appropriately predict its presence and control its level.

In a warm and wet climate, the most serious problems for a building caused by moisture are the ones arising from condensation. Condensation occurs when the water vapor pressure, at a certain point, exceeds the corresponding saturation vapor pressure for the temperature at that point and is classified into surface condensation and concealed condensation. Surface condensation can occur when a window has low airtightness, thereby letting outside air, which has higher humidity than inside air, enter the room in summer, while surface condensation occurs when the thermal insulation properties of a building's outer structures, including its external walls, roof and windows, are insufficient, lowering the surface temperature on the inside of the building in winter. Concealed condensation can occur when a wall has not been moisture-proofed, thereby allowing water vapor to encroach.

Condensation in buildings can induce the proliferation of microorganisms, such as molds and mites. Becker [1] conducted statistical analysis on condensation and mold growth in 200 dwellings with parameters, such as location and orientation of the dwelling, occupant density and type of finishing material, and showed that mold growth occurred mainly on the thermal bridges and in dwellings with walls facing northeast to northwest, where surface condensation was observed. Using simulation, Lawton et al. [2] showed that condensation is a significant factor in mold growth in houses. Small [3] pointed out that condensation is the one cause of mold growth and emphasized that control of moisture is the essential strategy to prevent mold growth. Lengsfeld et al. [4] investigated the correlation between condensation and algae growth on outer façades and reported that microbiological growth mostly occurred on northern-oriented façades and surface condensation caused by natural long wave irradiation was the main moisture source on the façade. Pasanen et al. [5] performed field measurements and determined that condensation promotes fungal growth in ducts, especially when ventilation is turned off during nights and weekends. Fisk et al. [6], Meyer et al. [7], Bush et al. [8] and Burge et al. [9] discussed the medical effects, such as respiratory illness, asthma, allergy, fatigue, headache and cutaneous disorder, on the human body when building occupants were exposed to microbial contamination. Mendell et al. [10], Maus et al. [11], Yanagi et al. [12] and the Occupational Safety and Health Administration (OSHA) of the U.S. [13] revealed facts about the microbial contamination in air-conditioning systems. When air-conditioning units or ducts were polluted by microbes, it was possible for contaminants to be resupplied to rooms.

Because the optimal growth environment (containment condition in inverse meaning) varies for each species of microbe, it is difficult to remove all microbes simultaneously and completely. In addition, if a microbe accrued in the building was not eradicated completely, its growth rate will increase rapidly when the indoor environment changes to the viable condition. Hence, it is necessary to take preventive measures to stop their initial growth.

For microbes to breed, they need nutrients, air, appropriate temperature and moisture. By controlling the indoor environment at conditions that are unfavorable to microbial growth, microbial growth can be contained. However, nutrients are ubiquitous in the environment, including because of an occupant's daily activities. In some cases, the building material itself becomes nutrients for microbes. Air is necessary for people's survival; therefore, it also cannot be removed from the building. In addition, as room temperature in daily use (approximately 15–30 °C) is the most conducive temperature for the growth of microbes, it would be difficult to try to control microbes by changing the temperature of the room. As a result, controlling moisture is essential to preventing the growth of microbes in buildings. In other words, to restrain the occurrence of microbes in a building, it is important to take measures to prevent condensation.

Condensation in a building induces not only harmful effects on an occupant's health, but also the deterioration of the building, such as rotteness of wooden building materials, decreased structural capacity in timber buildings, performance degradation of thermal insulation and discoloration or exfoliation of finishing materials [14–16].

Because it is difficult to take countermeasures to resolve condensation problems after building completion, the estimation of condensation considering the building's specifications and climate conditions is necessary from the design step of a construction process; i.e., where, when and why does condensation occur, and what can be done about it?

Janssens et al. [17] evaluated condensation due to the variation in air leakage in a lightweight roof system with a 2D heat, air and vapor transfer model and emphasized increasing the thermal resistance of the roof system and enhancing the removal of vapor from the inner surface of roof system to outside. Gutt [18] examined the validity of vapor barriers in an attic as a solution to condensation, pointed out that moisture moves into the attic mainly by airflow, not by diffusion, and proposed blocking airflow from living space to the attic as an effective anti-condensation measure. Bludau et al. [19] analyzed condensation in cool roofs, identified the effect of a roof surface's color on condensation and showed that a bright-colored roof can induce moisture accumulation in regions with very cold ambient

temperatures. Zillig et al. [20] and Sato et al. [21] evaluated the influence of a façade's material type on condensation and elucidated that a façade with low thermal resistance and large thermal capacity is advantageous in terms of anti-condensation, because the heat accumulated during the day in the façade's material and a larger scale of heat transmitted from the indoor environment reduce the effect of external night cooling. Aelemei et al. [22] investigated the effects of convection and the moisture content of outdoor air (OA) on condensation on building the façade and reported that the lower convective heat transfer coefficient of the façade, the higher the risk of surface condensation. Hien et al. [23] performed comparative analysis using computational fluid dynamics (CFD) simulation of single- and double-glazed façades in regards to energy consumption, thermal comfort and condensation and indicated that a double-glazed façade, which has the advantages of reducing the annual cooling loads and enhancing thermal comfort in the building, can promote condensation in the façade cavity, thereby requiring mechanical ventilation. Song et al. [24] conducted a case study of condensation evaluation on a double-glazed window system with an insulation spacer using 2D steady-state calculations and authenticated the effectiveness of the insulation spacer on inside surface condensation in a double-glazed window. Hamdan [25] examined condensation due to variations in insulation layer location and concluded that condensation may be decreased when the insulation layer is located at the interior side within the wall. Liu et al. [26] developed the 3D transient CFD model to estimate surface condensation on walls; the developed model can be used in the design for the position of the air inlet and the location of the exhaust fan. Ogniewicz et al. [27] analyzed condensation in porous insulation using steady-state calculations and demonstrated that condensation depends on the Péclet number, the Lewis number and the Biot number. Ge et al. [28] and Mumma [29] examined condensation in a chilled ceiling, and Muneer et al. [30] and Boyd et al. [31] developed software for evaluating condensation in buildings. Becker [32] compared the effect of heating patterns, such as intermittent or consecutive heating and the number of heating hours, on condensation, showed that consecutive heating is effective to prevent surface condensation and emphasized that the intensification of thermal insulation is essential, regardless of heating patterns. Mumovic et al. [33] evaluated the variations in condensation risk from steady-state and transient methods and indicated that the steady-state method can underestimate condensation risk, because of neglecting the diurnal fluctuations of the outdoor and indoor environmental conditions, as well as the transient response of the construction.

In most of the above-mentioned studies, standard floor, restricted zone or unitary wall configurations were used to determine condensation characteristics. However, even if microbial contamination occurs due to condensation in one of those targeted places, there is still a risk that it may spread throughout the building via the air-conditioning or by the buoyancy phenomenon. There is a high risk of microbial contamination spreading through the ducts and air-conditioning systems, resupplying microbes to the rooms, thereby spreading them throughout the building, especially in buildings employing a central air-conditioning system. In addition, the thermal environments on the top floor, which is affected heavily by solar radiation and ambient air, and the first floor, which is affected by heat loss from the soil, of the building are different from those on a standard floor. Thus, the conditions for condensation and the places where it is likely to occur may also differ. Therefore, it is advisable to determine condensation occurrence for all surfaces in the entire building. Furthermore, to consider the movements of airflow in the entire building and the effect of outdoor conditions, such as wind velocity, wind direction, wind pressure due to the height from the ground surface, infiltration and exfiltration, the airflow network should be coupled with a simulation to estimate condensation.

Most of the previous studies targeted specific indoor and outdoor conditions, e.g., midsummer and midwinter, and adopted steady-state simulation or short-term transient evaluation. However, when the air-conditioning system is turned off in winter, the temperatures of the wall surfaces drop, which allows condensation to form. Contrarily, in summer, condensation likely forms due to the infiltration of highly humid air from the outside. In other words, the causes of condensation vary for different seasons, making it essential to conduct evaluations throughout the year, including when the air-conditioning system is not being used.

Humidity fluctuation within a building is affected by the moisture adsorption-desorption properties of the building materials. Moreover, the humidity fluctuations within a room are affected greatly by the moisture adsorption-desorption of the papers kept in the room, of which there is likely to be a large quantity in an office building. It is necessary to consider the effects of their moisture adsorption-desorption when predicting humidity fluctuation in a building.

Based on the preceding background, condensation risk assessment for an office building was accomplished in the present study by performing the following processes.

- 1 By using TRNSYS simulation, condensation conditions for all wall surfaces in an office building were investigated to identify the location(s) where condensation occurred.
- 2 TRNFLOW was coupled to TRNSYS simulation to take into consideration the effect of air movements on condensation, e.g., supply air (SA), return air (RA) and exhaust air (EA) of the air-conditioning system; buoyancy due to variation in temperatures; infiltration and exfiltration.
- 3 Condensation risks were estimated throughout the year, including when the air-conditioning system was not in operation.
- 4 The adsorption-desorption of building materials, including papers in office building, was estimated.
- 5 An index for evaluating condensation risk was proposed that utilizes the condensation ratio (CR_t), condensation frequency (CF_n) and condensation risk (CR).
- 6 Furthermore, the effect of the airtightness of the window and variations in the thermal insulation properties of the external walls, roofs and windows, which are considered to affect the occurrence of condensation, on the CR were examined, and measures to restrain building condensation were discussed.

Condensation risk estimations in an office building were conducted under the condition of a warm and wet climate. As the representative city located in this climate, Tokyo, Japan, was selected. The detailed climate conditions of Tokyo are described in Section 2.1.1.

2. Condensation Risk Estimation under Reference Conditions

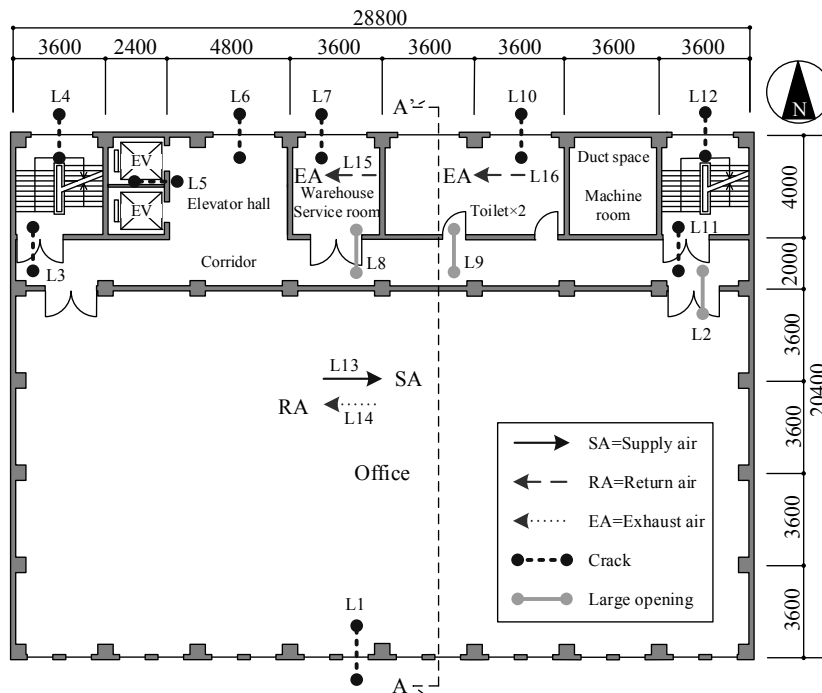
In this section, condensation estimation was performed for an office building located in Tokyo, Japan, under reference conditions, which satisfied the minimum standards of airtightness and thermal insulation; mass flow coefficient = $0.000250 \text{ kg}/(\text{s}\cdot\text{m})@1 \text{ Pa}$; thickness of thermal insulation (polystyrene foam type) for the external wall = 25 mm; thickness of thermal insulation (polystyrene foam type) for the roof = 50 mm; type of glass = single float.

2.1. Outline of Condensation Risk Estimation

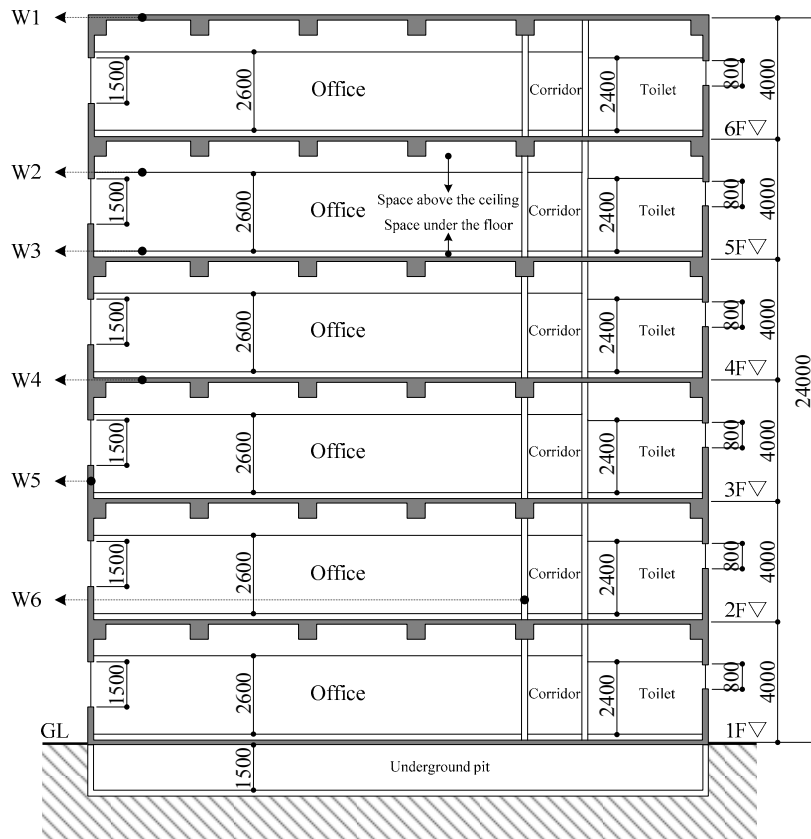
2.1.1. Analyzed Building Characteristics

Figure 1a shows the standard floor plan of the analyzed building, and Figure 1b shows the A-A' sectional view. The target building characteristics, a small-to-medium sized (six-story) office building located in Tokyo with a total floor area of 3525 m^2 , as proposed by Yuzawa et al. [34] were adopted.

Each of the rooms, as shown in the floor plan, was modeled as a zone, and the east and west staircases, elevator shaft and duct space and machine room were divided for each floor. In addition, the spaces under the floor and above the ceiling of the office each were modeled as a zone. Because of the input limitation for numbers of walls and airflows of TRNSYS and TRNFLOW, some rooms were simplified into one zone, e.g., warehouse and service room, toilets and duct space and machine room.



(a)

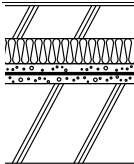
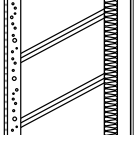


(b)

Figure 1. (a) Standard floor plan and airflow network of the analyzed building; (b) sectional view (A-A'). EV = elevator shaft; Ln = air link type number; Wn = wall type number. Figure unit = mm.

Table 1 shows the layer composition of each component making up the roof, external wall, floor, etc., and their corresponding heat transfer coefficients (U-factor). Table 2 shows the thermal property of each layer, e.g., thermal conductivity ($W/(m \cdot K)$); specific heat ($kJ/(kg \cdot K)$); density (kg/m^3). The specifications of the external wall and roof were set in accordance with the “Method for Calculations and Judgements in Conformity to the 2013 Building Energy Standard of Japan, Part 1. Non-Residential Buildings” [35]. The thickness of the thermal insulation materials (polystyrene foam type) was set to 25 mm for the external wall and 50 mm for the roof (see Table 12). Furthermore, a plan where the external wall was pasted on the outer surface of the pillars was assumed, and thus, the effects of a thermal bridge were not considered. The glazing of windows was set as single float glass (see Table 13). The ratio of the area on the façades occupied by windows was 20.8%.

Table 1. Heat transfer coefficient and layer composition of each wall type.

Wall Type (Wall Type Number ¹) (Heat Transfer Coefficient (U-Factor) ($W/(m^2 \cdot K)$))	Layer Composition (from Inner Side to Outer Side in the Zone), (Layer Thickness (mm))
Roof (W1) (0.611)	 Concrete (150), cement mortar (15), waterproofing layer (asphalt type, 5), cement mortar (15), thermal insulation material (polystyrene foam type, 50), concrete (60)
Ceiling (W2) (2.702)	 Acoustic board (12), gypsum board (10)
Raised floor (W3) (3.846)	 Carpet (3), aluminum type plate (10)
Floor (W4) (3.608)	 Concrete (150)
External wall (W5) (0.519)	 Gypsum board (8), non-closed air layer (-) ² , thermal insulation material (polystyrene foam type, 25), concrete (150), cement mortar (25), tile (10)
Internal wall (W6) (3.343)	 Gypsum board (24), non-closed air layer (-) ² , gypsum board (24)

¹ See Figure 1b for the numbers of the corresponding wall types; ² the thermal property of the non-closed air layer was set as thermal resistance ($=0.07 (m^2 \cdot K)/W$).

Table 2. Thermal property of each wall layer.

Material of Layer	Thermal Conductivity ($W/(m \cdot K)$)	Specific Heat ($kJ/(kg \cdot K)$)	Density (kg/m^3)
Concrete	1.40	0.88	2200
Cement mortar	1.5	0.80	2000
Waterproofing layer	0.110	0.92	1000
Polystyrene foam	0.040	1.13	20
Acoustic board	0.064	0.84	300
Gypsum board	0.70	1.0	910
Carpet	0.080	0.80	400
Aluminum type plate	210.0	0.88	2700
Tile	1.30	0.84	2400

The standard year weather data of the extended AMeDAS (Automated Meteorological Data Acquisition System) (1981–2000) for Tokyo [36] was used. Figure 2 shows the annual outdoor dry-bulb temperature ($^{\circ}C$) and humidity ratio (kg/kg dry air (DA)) of Tokyo. The ranges of outdoor dry-bulb

temperature and the humidity ratio of each air-conditioning period are summarized in Table 3. The maximum outdoor temperature and the mean outdoor temperature are 34.4 °C and 16.6 °C.

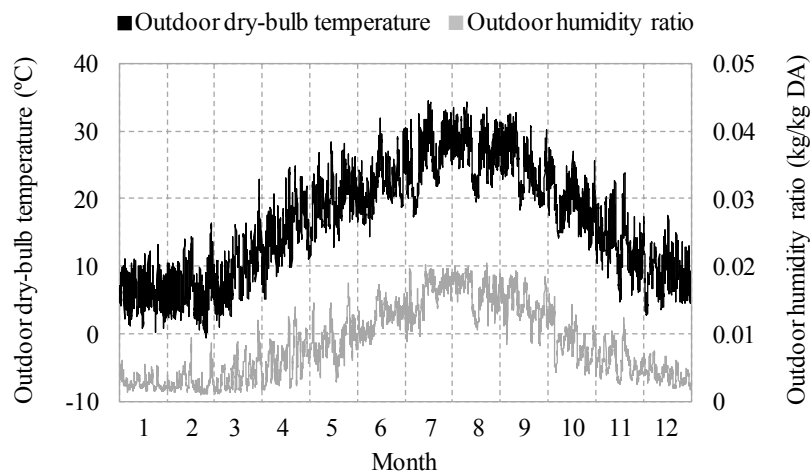


Figure 2. Annual outdoor dry-bulb temperature and humidity ratio of Tokyo. DA, dry air.

Table 3. Range of outdoor dry-bulb temperature and humidity ratio in each period.

Cooling Period (June–September)		Intermediate Periods (April–May and October–November)		Heating Period (December–March)	
Dry-bulb temperature (°C)	Humidity ratio (kg/kg DA)	Dry-bulb temperature (°C)	Humidity ratio (kg/kg DA)	Dry-bulb temperature (°C)	Humidity ratio (kg/kg DA)
14.4–34.4	0.0077~0.0204	−0.5~22.9	0.0010~0.0120	4.7~28.4	0.0017~0.0174

There was an underground pit 1.5 m deep underneath the first floor, and its external walls were set to be in contact with the ground. The ground temperature was calculated using Kusuda’s calculation method [37,38]. In Equation (1), mean ground temperature (it was substituted by using the mean annual ambient air temperature) T_{mean} (=16.6 °C), amplitude of surface temperature (maximum air temperature—minimum air temperature) T_{amp} (=17.8 °C) and day of the year corresponding to the minimum surface temperature t_{shift} (= 52) were calculated based on the weather data [36]. Thermal diffusivity of the ground (soil) α [39] was set to $1.4 \times 10^{-3} \text{ m}^2/\text{h}$.

$$T_{ground} = T_{mean} - T_{amp} \exp \left\{ -D \left(\frac{\pi \alpha}{365} \right)^{0.5} \right\} \cos \left[\frac{2\pi}{365} \left\{ t_{now} - t_{shift} - \frac{D}{2} \left(\frac{365\alpha}{\pi} \right)^{0.5} \right\} \right] \quad (1)$$

Figure 3 shows the results from calculating the ground temperature at a depth of 1.5 m and at the ground surface (depth = 0 m). The ground temperature at a depth of 1.5 m was lowest in early April due to the influence of the phase delay.

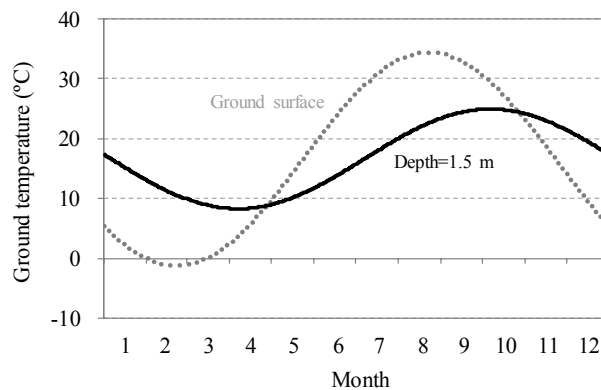


Figure 3. Ground temperature at a depth of 1.5 m and at the ground surface.

2.1.2. Internal Conditions in the Building

The air-conditioning on/off time, the internal heat generations, occupant density and air volume for ventilation were set based on the “Method for Calculations and Judgements in Conformity to the 2013 Building Energy Standard of Japan, Part 1. Non-Residential Buildings” [35].

Table 4 shows the air-conditioning period and each air-conditioning setting in an office. The air-conditioning system was operated from 7 a.m.–9 p.m. (preheating and precooling from 7 a.m.–8 a.m. and sensible heat load processing only for the offices) and only on weekdays, not on weekends or holidays.

Table 4. Air-conditioning setting in an office.

Summer (Cooling Period) (June–September)		Intermediate Periods (April–May and October–November)		Winter (Heating Period) (December–March)	
Dry-bulb temperature (°C)	Relative humidity (%)	Dry-bulb temperature (°C)	Relative humidity (%)	Dry-bulb temperature (°C)	Relative humidity (%)
26	50	24	50	22	50

The heat generated from the lighting and office application each was set at 12 W/m^2 and the occupant density at 0.1 person/m^2 , and these were multiplied by the ratios shown in Table 5. In addition, the ratios of heat generation from office appliances on weekends and holidays were set at 25% as a standby power condition. Based on the “Handbook of the Society of Heating, Air-Conditioning and Sanitary Engineers of Japan, Vol. 1 Fundamental” [40], the heat generated by a human body was set to be 121 W/m^2 , which was determined by dividing the proportion of sensible heat and latent heat for each set air-conditioning temperature. Table 6 shows heat generation from the human body by air-condition usage period. Furthermore, when calculating the water vapor emitted, only that generated by a human body was included, and the water vapor from the service rooms or toilets was not considered.

Table 5. Ratio of internal heat generation.

Time (h)	1	2	3	4	5	6	7	8	9	10	11	12
Lighting (%)	0	0	0	0	0	0	0	0	100	100	100	100
Office appliance (%)	25	25	25	25	25	25	25	25	100	100	100	100
Occupancy (%)	0	0	0	0	0	0	0	0	100	100	100	100

Table 5. Cont.

Time (h)	13	14	15	16	17	18	19	20	21	22	23	24
Lighting (%)	50	100	100	100	100	100	100	100	80	0	0	0
Office appliance (%)	80	100	100	100	100	100	100	50	50	25	25	25
Occupancy (%)	60	100	100	100	100	100	50	30	20	0	0	0

Table 6. Heat generation from a human body in an office.

Cooling Period (June–September)		Intermediate Periods (April–May and October–November)		Heating Period (December–March)	
Sensible heat (W)	Latent heat (W)	Sensible heat (W)	Latent heat (W)	Sensible heat (W)	Latent heat (W)
68	53	73	48	78	43

The air volume of ventilation in the offices was set as $5 \text{ m}^3/(\text{m}^2 \cdot \text{h})$. The ventilation in the toilets and warehouse/service room was set to occur at an air change rate (ACH) of five per hour, and part of the EA from the office was supplied via the corridor.

2.1.3. Airflow Network in the Building

The airflow networks for the standard floor plan were set as shown in Figure 1a, and Table 7 shows the air link types, from node to node, the areas of openings, the lengths of cracks, mass flow coefficients and airflow rate exponents. The airflow rate exponent of the window was set to one, in accordance with Japanese Industrial Standard (JIS) A 4706 [41]. The airflow rate exponent and mass flow coefficients of other air links were set to 0.6, based on the TRNFLOW manual [42].

In this study, not only the airflows of the plane, but also the airflows above and below the staircases and EV shafts were considered. An opening was classified as a large opening (LO) or crack according to TRNFLOW [42]. The doors of the offices had a door louver (600 mm × 300 mm, aperture ratio 40%), and the doors of the toilets, warehouses and service rooms had an undercut of 0.01 m. The door louvers and undercuts were classified as LOs, and the other gaps in the doors and windows were classified as cracks. The airtightness of a window was given an A-2 grade (for general building) as stipulated in JIS A 4706 [41] (see Table 11).

To consider the airflow within the building through the air-conditioning system, airflow networks, including SA, RA and EA of the air-conditioning system, were established as shown in Figure 1a. The SA and RA were set on the office ceiling, whereas the EA was set on the ceilings of the toilets and warehouses/service room zones. The SA was modeled with a fan, auxiliary node and duct according to TRNFLOW [42]. Airflow rate, dry-bulb temperature and relative humidity of the SA were calculated every hour, as explained below in Section 2.1.4. The fan was modeled to blow out this air volume, and the auxiliary node was used to define the temperature and humidity of the SA. In addition, the RA air volume was set with the fan, and the RA air volume in the office became the difference in the airflow rates of the SA in the office and the ventilation in the toilets and warehouse/service room zones.

Table 8 shows the wind pressure coefficient according to wind angle for each of the building's walls. Values that were interpolated linearly depending on the wind direction, by diverting the wind pressure coefficient of the eight directions used in a three-story square plane building located in a shielded area according to Table A3 of the TRNFLOW manual appendix [42], were used as the wind pressure coefficients. As the wind pressure coefficient value in the shielded category assumes that the surroundings are enclosed with buildings of the same type, its value is small as compared to the general single-structure locations. Furthermore, the wind pressure coefficient was set uniform, and its surface distribution was not considered.

Table 7. Setup of airflow links in standard floor. OA = outdoor air; SA = supply air; RA = return air; EA = exhaust air.

Air link Number ¹	From Node	To Node	Air Link Type	Characteristics of the Link
1	OA (south)	Office	Crack	Length of crack = 80 m; mass flow coefficient = 0.00025 kg/(s·m)@1 Pa; airflow exponent = 0.6
2	Office	Corridor	Large opening	Door louver; area of opening = 0.6 m (W) × 0.3 m (H); number of openings = 4; opening rate = 40 %; airflow exponent = 0.6
3	Elevator hall/corridor	Staircase (west)	Crack	Length of crack = 9.6 m; mass flow coefficient = 0.0000130 kg/(s·m)@1 Pa; airflow exponent = 0.6
4	Staircase (west)	OA (north)	Crack	Length of crack = 6.4 m; mass flow coefficient = 0.00025 kg/(s·m)@1 Pa; airflow exponent = 1
5	Elevator hall/corridor	Elevator shaft	Crack	Length of crack = 18 m; mass flow coefficient = 0.0000130 kg/(s·m)@1 Pa; airflow exponent = 0.6
6	Elevator hall/corridor	OA (north)	Crack	Length of crack = 6.4 m; mass flow coefficient = 0.00025 kg/(s·m)@1 Pa; airflow exponent = 1
7	Warehouse/service room	OA (north)	Crack	Length of crack = 6.4 m; mass flow coefficient = 0.00025 kg/(s·m)@1 Pa; airflow exponent = 1
8	Elevator hall/corridor	Warehouse/service room	Large opening	Undercut of door; area of undercut = 2 m (W) × 0.01 m (H); number of undercuts = 1; airflow exponent = 0.6
9	Elevator hall/corridor	Toilet	Large opening	Undercut of door; area of undercut = 0.9 m (W) × 0.01 m (H) ; number of undercuts = 2; airflow exponent = 0.6
10	Toilet	OA (north)	Crack	Length of crack = 12.8 m; mass flow coefficient = 0.00025 kg/(s·m)@1 Pa; airflow exponent = 1
11	Elevator hall/corridor	Staircase (east)	Crack	Length of crack = 9.6 m; mass flow coefficient = 0.0000130 kg/(s·m)@1 Pa; airflow exponent = 0.6
12	Staircase (east)	OA (north)	Crack	Length of crack = 6.4 m; mass flow coefficient = 0.00025 kg/(s·m)@1 Pa; airflow exponent = 1
13	Auxiliary node	Office	Duct	SA; dry-bulb temperature, humidity ratio and airflow rate of SA were set according to the calculation method described in Section 2.1.4
14	Office	Auxiliary node	Fan	RA; airflow rate = airflow rate of SA – airflow rate of EA
15	Warehouse/service room	Auxiliary node	Fan	EA; airflow rate = 5 ACH
16	Toilet	Auxiliary node	Fan	EA; airflow rate = 5 ACH

¹ See Figure 1a for the numbers of the corresponding air links.

Table 8. Wind pressure coefficient according to wind angle.

Wall Orientation	Wind Angle (South = 0°, West = 90°, North = 180°, East = 270°)							
	0°	45°	90°	135°	180°	225°	270°	315°
South	0.2	0.05	−0.25	−0.3	−0.25	−0.3	−0.25	0.05
West	−0.25	0.05	0.2	0.05	−0.25	−0.3	−0.25	−0.3
North	−0.25	−0.3	−0.25	0.05	0.2	0.05	−0.25	−0.3
East	−0.25	−0.3	−0.25	−0.3	−0.25	0.05	0.2	0.05

2.1.4. Supply Air Condition of Air-Conditioning

The air-conditioning system was set as a single duct variable air volume (VAV) system. The SA condition was modeled based on the load calculation results. Using the sensible-heat load for every hour in the offices on every floor, the SA air volume V_{SA} was calculated using Equation (2).

$$V_{SA} = \frac{q_{SH}}{c_A \rho_A \Delta T_{Office_SA}} \quad (2)$$

The SA temperature and humidity conditions during the cooling period were 16 °C and 90%, respectively, and any OA introduced above the minimum volume (= 2073.6 m³/(h·floor)) was always blown out. For all of the offices on Floors 1–6, when the minimum volume of OA was introduced, the SA temperature was calculated backward from Equation (2). The humidity ratio at this time adopted the small value of water vapor from the relative humidity of 90% and the outlet of the enthalpy recovery ventilator (ERV). The outlet temperature (°C) of ERV T_{ERV} was calculated from Equation (3) and the humidity ratio (kg/kg DA) of the ERV X_{ERV} from Equation (4). Both the sensible-heat exchange efficiency η_{SH} (–) and the latent-heat exchange efficiency η_{LH} (–) of the ERV were set as 0.7.

$$T_{ERV} = T_{OA} - \eta_{SH}(T_{RA} - T_{OA}) \quad (3)$$

$$X_{ERV} = X_{OA} - \eta_{LH}(X_{RA} - X_{OA}) \quad (4)$$

For the heating period, the SA volume was calculated from Equation (2), setting the difference in temperature between the office and SA ΔT_{Office_SA} to be 10 °C. Furthermore, using the latent-heat load of the office, the SA humidity ratio X_{SA_Humid} (kg/kgDA) was calculated from Equation (5).

$$X_{SA_Humid} = X_{SP_Humid} - \frac{q_{LH}}{\rho_A L V_{SA}} \quad (5)$$

2.1.5. Moisture Adsorption-Desorption of Building Materials

The Buffer Storage Humidity Model (Moisture Capacitance Model) [43–47] of TRNSYS was used to calculate the moisture adsorption-desorption of the building materials. This model can be used to calculate the moisture migration between the zone and the surface of a building material and between the surface of a building material and the deep portions of a building material (Figure 4). In Equation (6), the zone humidity was calculated, considering the exchange of moisture between the zone node and the surface storage. The dynamics of the water content of the surface storage and deep storage were calculated using Equations (7) and (8), respectively.

Not only was the moisture adsorption-desorption of the building materials considered, but also that of the papers in the offices. The amount of papers stored inside the offices was quoted from actual survey results [48] and set to 5.7 fm/person. The unit fm means the height (m: meter) of the cumulated A4 size (210 mm × 297 mm) papers. Because the maximum number of occupant in this office building is 41 persons/floor, the total amount of papers is 14.60 m³/floor. The total surface area of papers was calculated assuming that papers occupied 25% of the desk surface area. These papers were modeled as one part of the walls in the simulations. Table 9 shows the moisture adsorption-desorption property of the building materials, as well as one piece of paper. These properties were set based on the

Japanese database (materials) in WUFI pro 4.2. The values in database were estimated by Japan Testing Center for Construction Materials (JTCCM). Adsorption isotherms of the database were measured under the condition that the temperature in the desiccator was controlled at 23 °C, according to JIS A 1475 [49]. Assuming that indoor relative humidity was in the range of 40%–60%, the gradients of sorptive isothermal lines in Table 9 were calculated from the gradient of the straight line connecting two moisture contents ((kg (water)/kg (building material)) of relative humidity of 40% and 60% on adsorption isotherms. The adsorption process and desorption process have different curves on the adsorption isotherm; this characteristic is called hysteresis. However, the adsorption-desorption calculation in the Buffer Storage Humidity Model uses the same curves. In other words, the desorption process is treated as the adversarial process of adsorption. The fluctuations of adsorption-desorption due to variations in indoor air temperature and building material's temperature are not considered in the Buffer Storage Humidity Model.

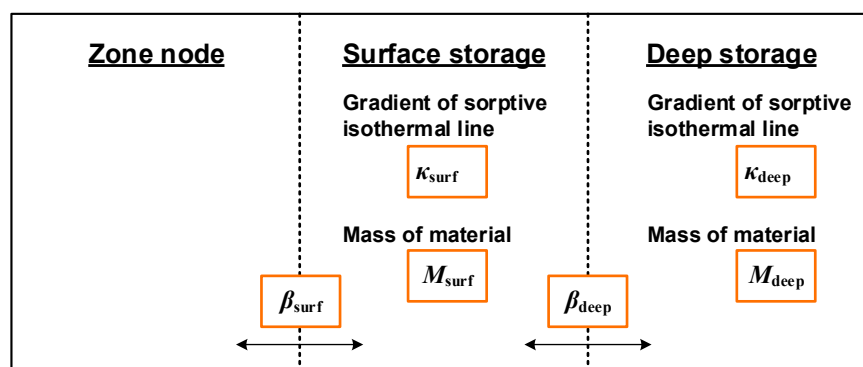


Figure 4. Conceptual diagram of the Buffer Storage Humidity Model.

$$M_{air,i} \frac{d\omega_i}{dt} = \dot{m}_{inf,i}(\omega_a - \omega_i) + \sum_k^{nvent} \dot{m}_{v,k,i}(\omega_{v,k,i} - \omega_i) + \dot{W}_{g,i} + \sum_c^{nlink} \dot{m}_{l,c,i}(\omega_{l,c,i} - \omega_i) + \beta_{surf}(\omega_{surf} - \omega_i) \quad (6)$$

$$M_{surf} \kappa_{surf} f(\varphi, \omega) \frac{d\omega_{surf}}{dt} = \beta_{surf}(\omega_i - \omega_{surf}) + \beta_{deep}(\omega_{deep} - \omega_{surf}) \quad (7)$$

$$M_{deep} \kappa_{deep} f(\varphi, \omega) \frac{d\omega_{deep}}{dt} = \beta_{deep}(\omega_{surf} - \omega_{deep}) \quad (8)$$

Table 9. Properties of building materials for the Buffer Storage Humidity Model.

Building Materials and Paper	Density (kg/m ³)	Gradient of Sorptive Isothermal Line ((kg (Water)/kg (Building Material))/(Relative Humidity))	Diffusion Resistance (–)
Acoustic board	300	0.013	1
Concrete	2200	0.040	70
Gypsum board	910	0.015	8
Cement mortar	2000	0.020	35
Polystyrene foam	20	0.700	50
Paper	100	0.120	53

Using the wall area shown in Figure 1, the thickness of each layer from Table 1, the thermal properties in Table 2 and the properties presented in Table 9, the parameters of the Buffer Storage Humidity Model for a standard floor were estimated (Table 10).

Table 10. Parameters setup of the Buffer Storage Humidity Model for a standard floor.

Zone	Surface Buffer Storage			Deep Buffer Storage		
	β_{surf}^1	κ_{surf}^2	M_{surf}^3	β_{deep}^1	κ_{deep}^2	M_{deep}^3
Office	2444.2	0.016	2660.4	814.7	1	7326.7
Elevator hall/corridor	258.7	0.015	497.4	86.2	1	753.1
Staircase (east, west)	175.9	0.033	1239.3	58.6	1	551.6
Elevator shaft	113.8	0.015	344.2	37.9	1	151.0
Warehouse/service room	152.2	0.015	331.7	50.7	1	380.3
Toilets	258.7	0.015	497.4	86.2	1	753.1
Duct space/machine room	174.7	0.037	2755.1	58.2	1	305.2

¹ The unit of β_{surf} and β_{deep} is kg (air)/h; ² the unit of κ_{surf} and κ_{deep} is (kg (water)/kg (building material))/(relative humidity); ³ the unit of M_{surf} and M_{deep} is kg (building material)/h.

As shown in Table 9, compared to the moisture diffusion resistance of air, that of building materials was 8–70-times greater; thus, the moisture adsorption-desorption occurred predominantly between the zone node and the surface storage. Furthermore, this study focused on condensation on wall surfaces, microbial viability due to condensation and the spreading of microbial contamination due to air movements; therefore, the estimation of condensation was targeted on only wall surfaces. In other words, concealed condensation was not considered.

2.1.6. Index of Condensation Risk

TRNSYS judges condensation based on the magnitude correlation of the surface temperature and the dew-point temperature of air. If condensation occurred on a wall surface, the judgement was one, and if not, the judgement was zero. This was only one way to determine whether or not condensation occurred; for example, it evaluated the condensation occurring on large surface areas, like the office floor area (414.72 m²), and that on small surface areas, like the windows in the core parts (1.92 m²), equally. Therefore, it was necessary that condensation on wall surfaces be estimated in consideration of the area of the wall surface. In this study, the three indicators of the condensation ratio, condensation frequency and condensation risk, as given below, were defined and evaluated.

By taking the area of a wall surface n ($= 1, 2, \dots, 452$ surfaces) as A_n and the occurrence (judgement = 1) or non-occurrence (judgement = 0) of condensation on the wall surface n during time step t ($= 1, 2, \dots, 8760$ hours) as $IC_{n,t}$, the condensation ratio CR_t in time t was defined using Equation (9); the condensation frequency CF_n for wall surface n was defined using Equation (10); and condensation risk CR throughout the year was defined using Equation (11).

$$CR_t = \frac{\sum_{n=1}^{452} IC_{n,t} A_n}{\sum_{n=1}^{452} A_n} \times 100 \quad (t = 1, 2, \dots, 8760) \quad (9)$$

$$CF_n = \frac{\sum_{t=0}^{8760} IC_{n,t}}{8760} \times 100 \quad (n = 1, 2, \dots, 452) \quad (10)$$

$$CR = \frac{\sum_{n=1}^{452} CF_n A_n}{\sum_{n=1}^{452} A_n} \quad (11)$$

The CR_t is an indicator that expresses the ratio of wall area where condensation has occurred to total wall area in the building and has one value for each time step. The CF_n is an indicator that expresses the ratio of total hours when condensation has occurred to the 8760 h (one year) for wall

surface n in the building and has 452 values for each time step. The CR is an indicator calculated from the areal mean CF_n of all wall surfaces in the building and has one value for the entire building for the year. The summation of A_n , total area of 452 surfaces, is 10,980.3 m².

2.2. Results and Discussion of Condensation Risk Estimation under Reference Conditions

Figure 5 shows the CR_t throughout the year. The maximum CR_t occurred on December 6 at 7 a.m., and the CR for the year was 0.353%. Most of the condensation occurred in winter (December–March). Compared to the CR_t in winter, although the value is very small, condensation also occurred in the intermediate periods (April and October–November).

Figure 6 shows the CR for each floor. The risk was highest for the topmost floor. Because the roof of the top floor is exposed to OA of low temperature in winter, the surface temperature of the roof tends to decrease easily, which can induce condensation on the wall surfaces. Therefore, it was concluded that intensifying the performance of thermal insulation of the roof would reduce CR s effectively.

Figure 7 shows the CR_t of the day when it was at its maximum and before and after three days. Most of the condensation that occurred in the offices happened when the air-conditioning system was not in operation, and there was minimal condensation when the air-conditioning system was running. Moreover, even when the air-conditioning system was not in operation, condensation occurrence was markedly less as compared to the core parts. Thus, the condensation countermeasures in non-air-conditioned core parts are key points for the restriction of condensation problems in the entire building.

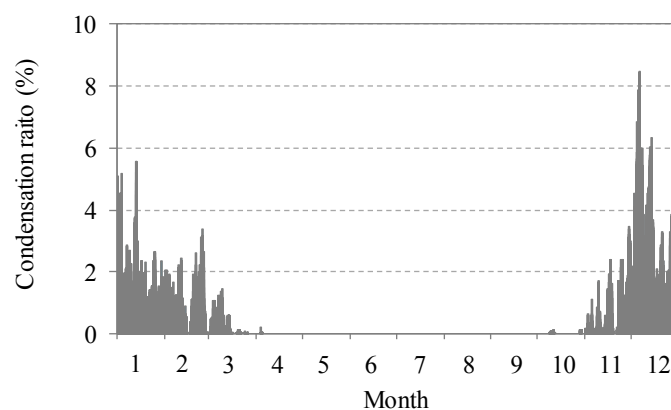


Figure 5. Annual condensation ratio.

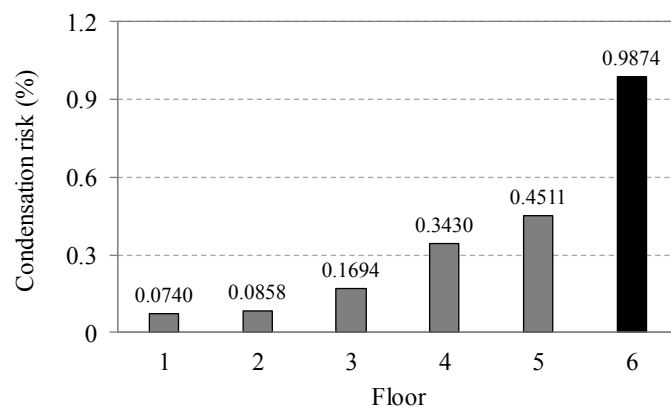


Figure 6. Condensation risk for each floor.

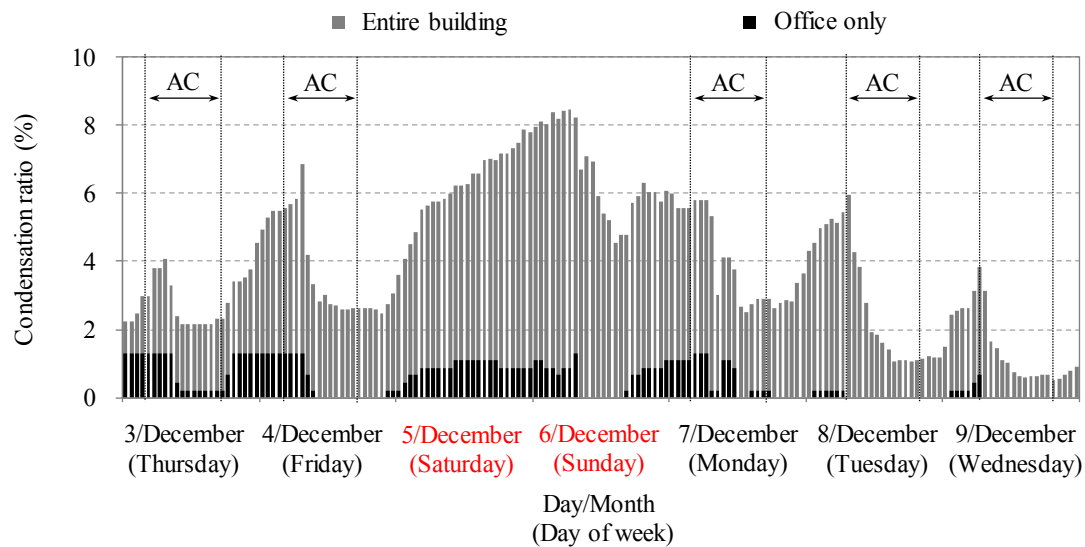


Figure 7. Condensation ratio in a week (December 3–December 9). AC = air-conditioning on.

3. Condensation Risk Estimations under Varying Airtightness Conditions

In this section, the influence of variations in the airtightness of windows on condensation and a method to restrain such condensation are discussed.

3.1. Case Setup for Airtightness

Thermal insulation specifications of the external walls, roof and windows were fixed to the reference conditions mentioned in Section 2.1. In accordance with the airtightness grade stipulated in JIS A 4706 [41], the assessment of CR was conducted by changing the airtightness of the windows in the offices and core parts. Table 11 shows a summary of the airtightness grades according to JIS. The A-4 grade indicates the highest performance, with Grades A-3 A-2, and A-1 representing decreasing orders of airtightness performance.

Table 11. Airtightness of windows based on the Japanese Industrial Standard (JIS).

Grade	Criterion	Mass Flow Coefficient (kg/(s·m) ² @1 Pa)	Airflow Exponent (–)
A-1	Area where ventilation is required	0.001000	1
A-2 ¹	General building thermally-insulated or dust-proofed building	0.000250	1
A-3		0.000067	1
A-4		0.000017	1

¹ The grade of A-2 corresponds to the airtightness performance of the reference condition.

3.2. Results and Discussion of Condensation Risk Estimations for Airtightness

Figure 8 shows a scatter diagram with crack characteristic values of windows versus CR. The risks were lower for windows with lower airtightness grades. Figure 9 shows the mass flow rate of infiltration into the sixth floor of the east staircase, where the greatest condensation occurred on the day when the CR_t was at its maximum and before and after three days. Figure 10 shows the relative humidity in the same zone for the same days. It is clear from these figures that for lower airtightness grades, the amount of OA entering through the gaps of the window is greater, causing the relative humidity of the staircase to decrease. This effect results in reduced CRs for lower airtightness grades.

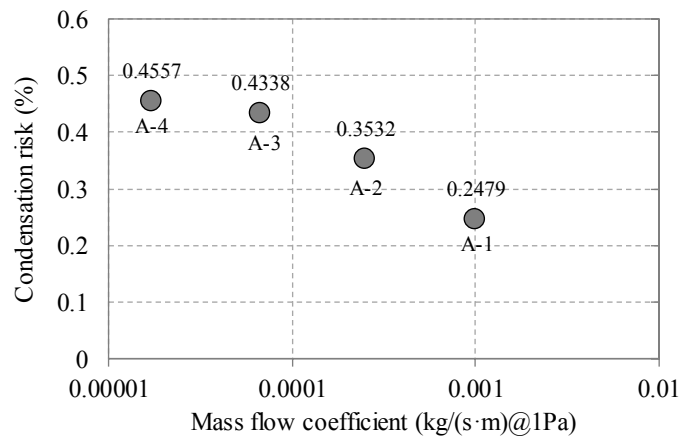


Figure 8. Condensation risk under varying airtightness conditions.

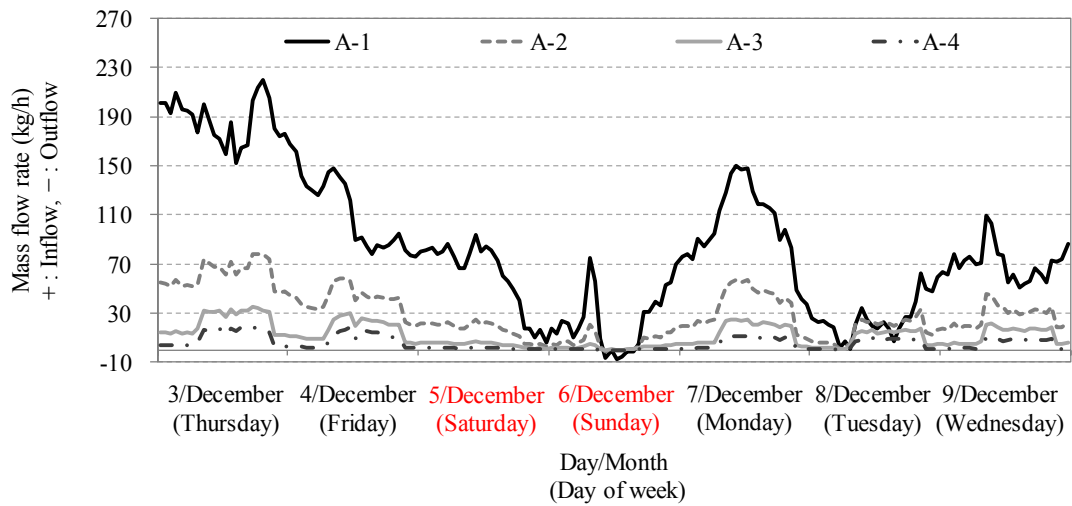


Figure 9. Mass flow rate of infiltration in the sixth floor of the east staircase (3 December–9 December).

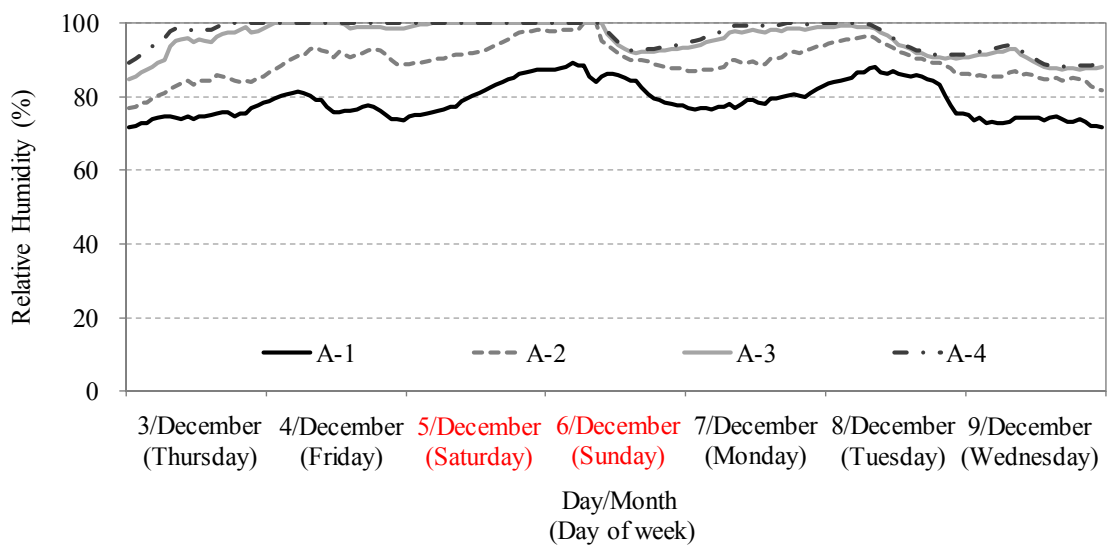


Figure 10. Relative humidity in the sixth floor of the east staircase (3 December–9 December).

Rather than follow the JIS standards for high airtightness that are effective at reducing air-conditioning load and improving soundproofing and dust-proofing, from the perspective of condensation reduction alone, CRs can be lowered with lower airtightness.

4. Condensation Risk Estimations under Varying Thermal Insulation Conditions

In this section, condensation estimations by varying the thermal insulation performance of external walls, roof and windows and the specifications of the thermal insulation of these building parts to restrain condensation completely were discussed. After examining the insulation thickness of the external walls, by varying the thermal insulation performance of roof and glass, condensation estimations were conducted to investigate the thermal insulation conditions needed to realize non-condensation in the building.

4.1. Condensation Risk Estimations for Thermal Insulation of External Walls

4.1.1. Case Setup for Thermal Insulation of External Walls

Table 12 shows the case study settings. Using the roof specifications (thermal insulation thickness: 50 mm) and window specifications (single float glass) from the reference conditions, a case study was performed by altering only the thickness of the external walls' thermal insulation (0–100 mm). Grade A-2 was the standard for airtightness when analyzing the thermal insulation changes.

Table 12. Variation in the thickness of thermal insulation of the external wall.

Thickness of Thermal Insulation (mm)	External Wall	0	5	15	25 ¹	50	75	100
		Roof	The thickness of thermal insulation in roof was fixed at 50 mm ²					
	Type of Glass	The type of glass was fixed at single float glass ³						

^{1, 2, 3} Reference conditions described in Section 2.1.

4.1.2. Results and Discussion of Condensation Risk Estimations for the Thermal Insulation of External Walls

Figure 11 shows the correlation between the thickness of thermal insulation of the external walls and the CR. The risk decreased as the thickness of the thermal insulation of the external walls increased. However, above a thickness of 50 mm, there was no significant change in the CR with an increase in thickness of the thermal insulation.

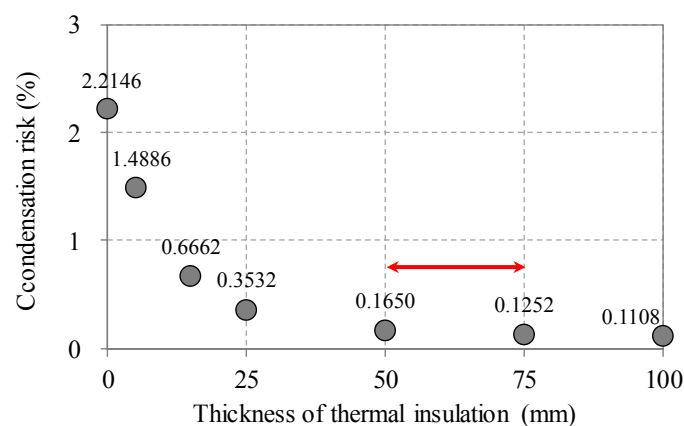


Figure 11. Condensation risk with different thicknesses of insulation of the external wall (0–100 mm).

Condensation in all areas below the fifth floor, except for the windows, was suppressed completely when the thickness of the thermal insulation was 75 mm. However, for the sixth floor, condensation was present not only on the windows, but also on the external walls and roof. The results were similar for 100 mm-thick thermal insulation. As mentioned in Section 2.2, improvement in thermal insulation of the roof is important for reducing CRs.

Detailed analysis was conducted by increasing the thermal insulation thickness of the external walls from 50 mm–75 mm, 5 mm at a time, and observing the exact thickness at which condensation failed to occur on all areas of Floors 1–5, except for the windows. Figure 12 shows the results of this detailed analysis. There was no considerable change in the CR of the building as a whole. The results also indicated that condensation failed to occur with a thickness of 75 mm on all areas of Floors 1–5, except the windows.

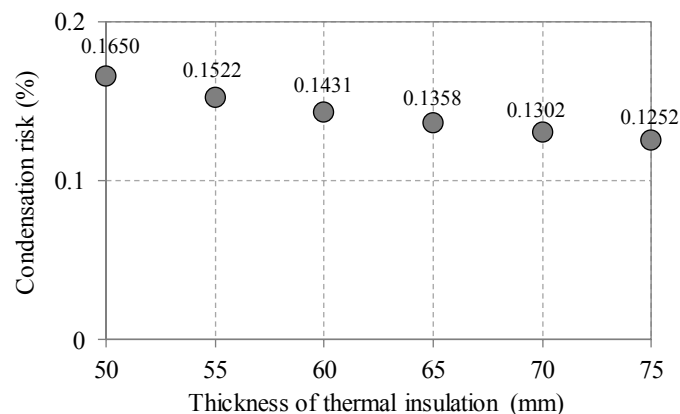


Figure 12. Condensation risk with different thicknesses of the insulation of the external wall (50–75 mm).

Increasing the thermal insulation thickness of the external walls to 75 mm completely suppressed condensation on all areas of Floors 1–5, except the windows, but condensation still occurred on the ceiling and external walls of the topmost floor. Even after increasing the thermal insulation material thickness of the external walls from 75 m–100 mm, condensation continued to occur on the topmost floor in places other than the windows. Furthermore, it caused no significant change in the CR of the building as a whole.

4.2. Condensation Risk Estimations for the Thermal Insulation of the Roof

4.2.1. Case Setup for the Thermal Insulation of the Roof

As the second step for reinforcement of thermal insulation, the thickness at which condensation on all areas of the topmost floor other than the windows was suppressed was investigated, by keeping the thermal insulation thickness of the external walls at 75 mm and the type of glasses at single float glass and increasing the thermal insulation thickness of the roof from 50 mm upwards, 5 mm at a time.

4.2.2. Results and Discussion of Condensation Risk Estimations for Thermal Insulation of Roof

As a result, condensation was suppressed completely on all areas of the topmost floor except the windows when the thermal insulation material thickness of the roof was 105 mm. The CR at this point was 0.109%.

Figure 13 shows the CF_n for the windows of each zone when the thermal insulation material thickness of the external walls was 75 mm and that of the rooftop was 105 mm. Although condensation on the external walls and roof was suppressed completely, there was still a large amount of condensation occurring on the windows, particularly in the core parts of Floors 4–6, where the

CF_n was above 10%, and the east staircase of the topmost floor, where condensation occurrence was greatest, at above 20%.

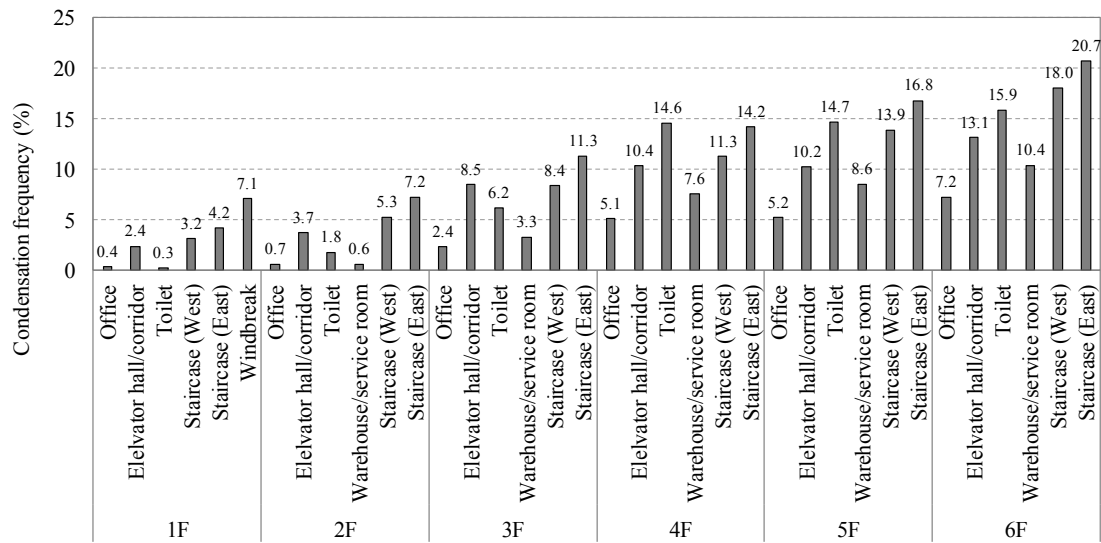


Figure 13. Condensation frequency for the windows in each zone (thermal insulation of external the wall = 75 mm, thermal insulation of the roof = 105 mm).

4.3. Condensation Risk Estimations for Thermal Insulation of Glass

4.3.1. Case Setup for Thermal Insulation of Glass

From the results in the Sections 4.1 and 4.2, it can be concluded that improving the thermal insulation of the windows was particularly important, making it essential to take countermeasures. For this reason, the thermal insulation performance of glass was enhanced until condensation stopped occurring on them. Thus, by intensifying the thermal insulation performance of windows as shown in Table 13, condensation estimations were carried out. The thermal insulation thickness of the external walls and the roof were fixed at 75 mm and 105 mm.

Table 13. Enhancement of the thermal insulation performance of glass.

Type of Glass	U-Factor (W/(m ² ·K))	Solar Heat Gain Coefficient (–)	Shading Coefficient (–)	Frame
Single float ¹	5.53	0.797	0.78	Aluminum type; area ratio of frame to window = 0.15; solar absorptance = 0.6; U-factor = 2.27 W/(m ² ·K)
Double float	3.35	0.782	0.91	
Double low-e	2.53	0.567	0.66	
Triple float	2.00	0.700	0.78	

¹ Single float glass corresponds to the thermal insulation performance of the reference condition.

4.3.2. Results and Discussion of Condensation Risk Estimations for Thermal Insulation of Glass

Figure 14 shows a scatter diagram with the U-factor of the windows versus the CR. Although several values could be used as indicators of window performance, the U-factor was selected, as correlation with the CR is considered to be dependent mainly on the U-factor. As a result, even double low-e glass could not eliminate condensation. It was not until the adoption of the triple float glass (U-factor = 2.0 W/(m²·K)) that condensation was completely suppressed in the entire building.

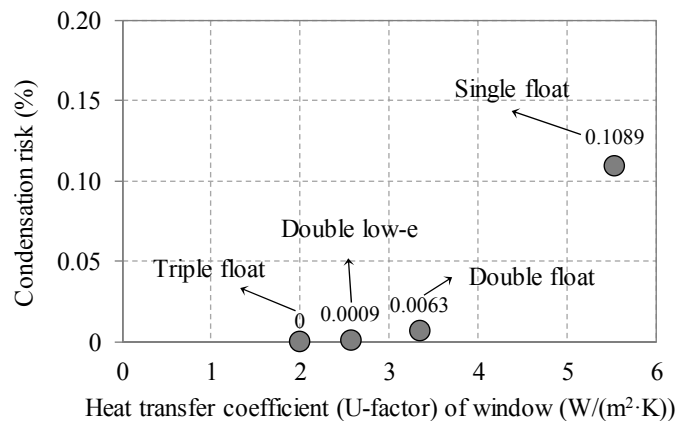


Figure 14. Heat transfer coefficients (U-factors) of windows and condensation risk (thermal insulation of external the wall = 75 mm, thermal insulation of the roof = 105 mm).

It is not possible to control the generation of water vapor inside the office building, as the exhalation of the occupants is a source of water vapor. Therefore, regarding the factors for condensation occurrence in winter, the only way to restrain condensation is by controlling the drop in wall surface temperature, or in other words, by increasing the thermal insulation performance of the walls.

5. Conclusions

In this study, a CR assessment of the entire office building was conducted throughout the year, including when the air-conditioning system was not in operation, by considering the heat transfer between zones, the absorption-desorption properties of the building materials and papers stored in the rooms and the air movements within the entire building. Furthermore, an analysis to identify the impact of variations in the thermal insulation of the external walls, roof and windows and airtightness of windows on CRs was performed, with the aim of controlling CRs. The results of this study are as follows:

- 1 Most of the condensation occurred in winter (December–March) with minimal condensation occurring in the intermediate periods (April–May and October–November).
- 2 For the topmost floor, because the roof surface is in contact with the OA during winter, the surface temperature of the roof tends to decrease easily, resulting in condensation. Therefore, improving the thermal insulation of the roof would be effective in reducing CRs.
- 3 The occurrence of condensation was significantly less in air-conditioned offices as compared to non-air-conditioned core parts. Thus, it can be concluded that the condensation countermeasures in non-air-conditioned core parts are important for the restriction of condensation within the entire building.
- 4 From the perspective of air-conditioning load, soundproofing and dust-proofing measures, the use of a highly airtight window was more helpful than the JIS standards. However, from the perspective of condensation reduction, when the airtightness of a window was of a lower grade, the humidity ratio of the rooms in winter decreased due to the infiltration of outside air containing less water vapor than the inside air, which resulted in lowered CRs.
- 5 Using thermal insulation materials 75 mm thick on the external walls completely suppressed condensation on all areas of Floors 1–5 except the windows, but it still occurred on the ceiling and external walls of the topmost floor. Even after increasing the thermal insulation material thickness of the external walls from 75 mm–100 mm, condensation continued to occur on the topmost floor on the windows, as well as other areas, necessitating an increase in the thickness of the thermal insulation materials of the roof. The thickness at which condensation was suppressed completely on all areas of the topmost floor except the windows was investigated, by keeping the

thermal insulation material thickness of the external walls at 75 mm and increasing the thickness of the materials of the roof from 50 mm upwards. By increasing the thickness up to 105 mm, condensation was suppressed completely throughout the building except for on the windows. However, a large amount of condensation occurred on the windows, making it necessary to improve their thermal insulation performance. Therefore, enhancement of thermal insulation is essential for suppressing condensation, especially of the roof and windows.

- 6 For the building in Tokyo that was the subject of this study, condensation within the building was suppressed completely when the thermal insulation material thickness of the external walls was greater than 75 mm, that of the roof was greater than 105 mm and the windows had triple float glass (U-factor: $2.0 \text{ W}/(\text{m}^2 \cdot \text{K})$) or better.

Future studies may focus on the CR assessment based on variations in the orientation of the buildings and the location of core parts and whether the windows are open or closed. Furthermore, as the present study focused on only one area and one building, similar studies on buildings of different sizes or in areas with different weather conditions should be conducted. Investigations into the correlation between CR and air-conditioning load and condensation within air-conditioning units are also necessary.

Acknowledgments: The authors would like to thank Shouhei Teranishi of the Shin Nippon Air Technologies Co., LTD. He contributed to one part of the simulation setup and subsequent data analysis during a master's course at Kanagawa University.

Author Contributions: Wanghee Cho performed the simulations, analyzed the simulation results and wrote the paper. Shizuo Iwamoto designed the simulations. Shinsuke Kato reviewed the paper. All authors have read and approved the final manuscript.

Conflicts of Interest: The authors declare no conflict of interest.

Abbreviation

The following abbreviations are used in this manuscript:

T_{ground}	Ground temperature, °C
T_{mean}	Mean ground temperature (average air temperature), °C
T_{amp}	Amplitude of surface temperature (maximum air temperature–minimum air temperature), °C
D	Depth below surface, m
α	Thermal diffusivity of the ground (soil), m^2/h
t_{now}	Current day of the year, 1, 2, . . . , 365
t_{shift}	Day of the year corresponding to the minimum surface temperature, 1, 2, . . . , 365
V_{SA}	Airflow rate of supply air, m^3/h
q_{SH}	Sensible-heat load of the office, kJ/h
c_A	Specific heat of air, $\text{kJ}/(\text{kg} \cdot \text{K})$
ρ_A	Density of air, kg/m^3
ΔT_{Office_SA}	Difference in temperature between the office and SA, °C
T_{ERV}	Outlet temperature of the enthalpy recovery ventilator, °C
T_{OA}	Temperature of outdoor air, °C
η_{SH}	Sensible-heat exchange efficiency of the enthalpy recovery ventilator, dimensionless value
T_{RA}	Temperature of return air, °C
X_{ERV}	Humidity ratio of the enthalpy recovery ventilator, kg/kg dry air
X_{OA}	Humidity ratio of outdoor air, kg/kg dry air
η_{LH}	Latent-heat exchange efficiency of the enthalpy recovery ventilator, dimensionless value

X_{RA}	Humidity ratio of return air, kg/kg dry air
X_{SP_Humid}	Humidity ratio of set-point for humidification, kg/kg dry air
q_{LH}	Latent-heat load of the office, kJ/h
L	Latent-heat of vaporization (kJ/kg)
$M_{air,i}$	Mass of air in zone i , kg
ω_i	Humidity ratio of zone i , kg/kg dry air
t	Elapsed time, h
$\dot{m}_{inf,i}$	Mass flow rate of infiltration, kg/h
ω_a	Ambient humidity ratio, kg/kg dry air
$\dot{m}_{v,k,I}$	Mass flow rate of ventilation type k , kg/h
$\omega_{v,k,i}$	Humidity ratio of ventilation type k , kg/kg dry air
$\dot{W}_{g,i}$	Internal moisture gains, kg/h
$\dot{m}_{l,c,i}$	Mass flow rate of air link type c , kg/h
$\omega_{l,c,i}$	Humidity ratio of air link type c , kg/kg dry air
β_{surf}	Mass transfer coefficient of surface storage, kg (air)/h
ω_{surf}	Humidity ratio of surface storage, kg/kg dry air
M_{surf}	Mass of surface storage, kg
κ_{surf}	Gradient of sorptive isothermal line of surface storage, (kg (water)/kg (building material))/(relative humidity)
$f(\varphi,\omega)$	Conversion factor from relative humidity to humidity ratio
β_{deep}	Mass transfer coefficient of deep storage, kg (air)/h
ω_{deep}	Humidity ratio of deep storage, kg/kg dry air
M_{deep}	Mass of deep storage, kg
κ_{deep}	Gradient of sorptive isothermal line of deep storage, (kg (water)/kg (building material))/(relative humidity)
CR_t	Condensation ratio during time-step t , %
$IC_{n,t}$	Occurrence or non-occurrence of condensation on wall surface n during time-step t , one or zero
A_n	Area of a wall surface n , m ²
CF_n	Condensation frequency for wall surface n , %
CR	Condensation risk, %

References

1. Becker, R. Condensation and mould growth in dwellings—Parametric and field study. *Build. Environ.* **1984**, *19*, 243–250. [[CrossRef](#)]
2. Lawton, M.D.; Dales, R.E.; White, J. The influence of house characteristics in a Canadian community on microbiological contamination. *Indoor Air* **1998**, *8*, 2–11. [[CrossRef](#)]
3. Small, B.M. Creating mold-free buildings: A key to avoiding health effects of indoor molds. *Arch. Environ. Health Int. J.* **2003**, *58*, 523–527. [[CrossRef](#)] [[PubMed](#)]
4. Lengsfeld, K.; Krus, M. Microorganisms on Facades—Reasons, Consequences and Measures. Available online: <http://www.kuleuven.be/bwf/projects/annex41/protected/data/FhG%20Oct%202004%20Paper%20A41-T3-D-04-5.pdf> (accessed on 18 January 2016).
5. Pasanen, P.; Pasanen, A.L.; Jantunen, M. Water condensation promotes fungal growth in ventilation ducts. *Indoor Air* **1993**, *3*, 106–112. [[CrossRef](#)]
6. Fisk, W.J.; Lei-Gomez, Q.; Mendell, M.J. Meta-analyses of the associations of respiratory health effects with dampness and mold in homes. *Indoor Air* **2007**, *17*, 284–296. [[CrossRef](#)] [[PubMed](#)]
7. Meyer, H.W.; Würtz, H.; Valbjørn, O.; Sigsgaard, T.; Gyntelberg, F. Moulds and Health—An Epidemiological Study. In Proceedings of the 9th International Conference on Indoor Air Quality and Climate, Vol. III, Indoor Air 2002, The International Academy of Indoor Air Sciences, Monterey, CA, USA, 30 June–5 July 2002; pp. 394–397.

8. Bush, R.K.; Portnoy, J.M.; Saxon, A.; Terr, A.I.; Wood, R.A. The medical effects of mold exposure. *J. Allergy Clin. Immunol.* **2006**, *117*, 326–333. [[CrossRef](#)] [[PubMed](#)]
9. Burge, S.; Hedge, A.; Wilson, S.; Bass, J.H.; Robertson, A. Sick building syndrome: A study of 4373 office workers. *Ann. Occup. Hyg.* **1987**, *31*, 493–504. [[CrossRef](#)] [[PubMed](#)]
10. Mendell, M.J.; Lei-Gomez, Q.; Mirer, A.G.; Seppänen, O.; Brunner, G. Risk factors in heating, ventilating, and air-conditioning systems for occupant symptoms in US office buildings: The US EPA BASE study. *Indoor Air* **2008**, *18*, 301–316. [[CrossRef](#)] [[PubMed](#)]
11. Maus, R.; Goppelsröder, A.; Umhauer, H. Survival of bacterial and mold spores in air filter media. *Atmos. Environ.* **2001**, *35*, 105–113. [[CrossRef](#)]
12. Yanagi, U.; Ikeda, K. A study on the behavior and control of microbial contamination in an air conditioning system: Part 1—Growth environment and contamination status of microbes. *J. Environ. Eng. (Trans. AIJ)* **2005**, *7*, 49–56. (In Japanese)
13. Occupational Safety and Health Administration (OSHA). *Preventing Mold-Related Problems in the Indoor Workplace*. Washington, DC: U.S. Department of Labor, Occupational Safety and Health Administration; Report No.: 3304–04N; Occupational Safety and Health Administration (OSHA): Washington, DC, USA, 2006.
14. Saito, H.; Fukuda, K.; Sawachi, T. Integration Model of Hygrothermal Analysis with Decay Process for Durability Assessment of Building Envelopes. In *Building Simulation*; Tsinghua Press: Beijing, China, 2012; Volume 5, pp. 315–324.
15. Andrade, C.; Sarría, J.; Alonso, C. Relative humidity in the interior of concrete exposed to natural and artificial weathering. *Cem. Concr. Res.* **1999**, *29*, 1249–1259. [[CrossRef](#)]
16. Vafai, K.; Sarkar, S. Condensation effects in a fibrous insulation slab. *J. Heat Transf.* **1986**, *108*, 667–675. [[CrossRef](#)]
17. Janssens, A.; Hens, H. Interstitial condensation due to air leakage: A sensitivity analysis. *J. Therm. Envel. Build. Sci.* **2003**, *27*, 15–29. [[CrossRef](#)]
18. Gutt, G.S. Condensation in attics: Are vapor barriers really the answer? *Energy Build.* **1979**, *2*, 251–258. [[CrossRef](#)]
19. Bludau, C.; Zirkelbach, D.; Künzle, H.M. Condensation problems in cool roofs. *Interface J. RCI* **2009**, *27*, 11–16.
20. Zillig, W.; Lenz, K.; Sedlbauer, K.; Krus, M. Condensation on Facades—Influence of Construction Type and Orientation. In Proceedings of the 2nd International Conference on Building Physics, Leuven, Belgium, 14–18 September 2003; pp. 437–444.
21. Sato, N.M.N.; Shirakawa, M.A.; Loh, K.; John, V.M. Influence of Thermal Properties of Materials in Condensation and Microorganism Growth on Building Façades. In Proceedings of the 11DBMC International Conference on Durability of Building Materials and Components, Istanbul, Turkey, 11–14 May 2008; pp. 11–14.
22. Aelenei, D.; Henriques, F.M.A. Analysis of the condensation risk on exterior surface of building envelopes. *Energy Build.* **2008**, *40*, 1866–1871. [[CrossRef](#)]
23. Hien, W.N.; Liping, W.; Chandra, A.N.; Pandey, A.R.; Xiaolin, W. Effects of double glazed facade on energy consumption, thermal comfort and condensation for a typical office building in Singapore. *Energy Build.* **2005**, *37*, 563–572. [[CrossRef](#)]
24. Song, S.Y.; Jo, J.H.; Yeo, M.S.; Kim, Y.D.; Song, K.D. Evaluation of inside surface condensation in double glazing window system with insulation spacer: A case study of residential complex. *Build. Environ.* **2007**, *42*, 940–950. [[CrossRef](#)]
25. Hamdan, M.A. Layered wall design to prevent moisture condensation on its inside surface. *Energ. Convers. Manag.* **2002**, *43*, 1821–1828. [[CrossRef](#)]
26. Liu, J.; Aizawa, H.; Yoshino, H. CFD prediction of surface condensation on walls and its experimental validation. *Build. Environ.* **2004**, *39*, 905–911. [[CrossRef](#)]
27. Ogniewicz, Y.; Tien, C.L. Analysis of condensation in porous insulation. *Int. J. Heat Mass Transf.* **1981**, *24*, 421–429. [[CrossRef](#)]
28. Ge, G.; Xiao, F.; Wang, S. Neural network based prediction method for preventing condensation in chilled ceiling systems. *Energy Build.* **2012**, *45*, 290–298. [[CrossRef](#)]
29. Mumma, S.A. Chilled ceilings in parallel with dedicated outdoor air systems: Addressing the concerns of condensation, capacity, and cost. *ASHRAE Trans.* **2002**, *108*, 220.

30. Muneer, T.; Abodahab, N. Frequency of condensation occurrence on double-glazing in the United Kingdom. *Energy Convers. Manag.* **1998**, *39*, 717–726. [[CrossRef](#)]
31. Boyd, D.; Cooper, P.; Oreszczyn, T. Condensation risk prediction: Addition of a condensation model to BREDEM. *Build. Serv. Eng. Res. Technol.* **1988**, *9*, 117–125. [[CrossRef](#)]
32. Becker, R. Effects of heating patterns on internal surface temperatures and risk of condensation. *Build. Environ.* **1993**, *28*, 333–345. [[CrossRef](#)]
33. Mumovic, D.; Ridley, I.; Oreszczyn, T.; Davies, M. Condensation risk: comparison of steady-state and transient methods. *Build. Serv. Eng. Res. Technol.* **2006**, *27*, 219–233. [[CrossRef](#)]
34. Yuzawa, H.; Sugihara, Y.; Kondo, T.; Hayashi, T.; Sekine, K.; Kohno, H.; Matsunawa, K.; Kato, S. Development of the Liquid Cooling Air-Conditioning System for Commercial Buildings (Part 2) Modeling of the Building and Air-Conditioning System for Feasibility Study. In Proceedings of the Society of Heating, Air-Conditioning and Sanitary Engineers of Japan, Nagano, Japan, 25–27 September 2013; pp. 21–24. (In Japanese)
35. Method for Calculations and Judgements in Conformity to the 2013 Building Energy Standard of Japan, Part 1. In *Non-Residential Buildings*, 1st ed.; National Institute for Land and Infrastructure Management and Building Research Institute, Rengo printing center Co., Ltd.: Tokyo, Japan, 2013; pp. 118–128. (In Japanese)
36. Architectural Institute of Japan. *Expanded AMeDAS Weather Data (1981–2000)*; Architectural Institute of Japan: Minato-ku, Tokyo, Japan, 2005.
37. Kusuda, T.; Achenbach, P.R. *Earth Temperature and Thermal Diffusivity at Selected Stations in the United States (No. NBS-8972)*; National Bureau of Standards Gaithersburg: Gaithersburg, MD, USA, 1965.
38. Thermal Energy System Specialist (TESS) Library Documentation. *The Ground Source Heat Pump Component Library, Type501 GROUND TEMPERATURE PROFILE*; Thermal Energy System Specialist (TESS): Madison, WI, USA, 2004.
39. Bureau of Construction, Tokyo Metropolitan Government, Ground of Tokyo (GIS version). Available online: <http://www.kensetsu.metro.tokyo.jp/jigyo/tech/start/03-jyouhou/geo-web/00-index.html> (accessed on 20 December 2015).
40. The Society of Heating, Air-Conditioning and Sanitary Engineers of Japan. *The handbook of the Society of Heating, Air-Conditioning and Sanitary Engineers of Japan, Vol.1 Fundamental*, 14th ed.; The Society of Heating, Air-Conditioning and Sanitary Engineers of Japan, Maruzen publishing Co., Ltd.: Tokyo, Japan, 2010; p. 414. (In Japanese)
41. Japanese Standards Association. *Japanese Industrial Standard Committee, JIS A 4706 Windows*; Japanese standards Association: Mita, Minato-ku, Tokyo, Japan, 2000.
42. Solar Energy Laboratory, Univ. of Wisconsin-Madison; TRANSSOLAR Energietechnik GmbH; CSTB—Centre Scientifique et Technique de Bâtiment; TESS—Thermal Energy System Specialists, LLC. *TRNFLOW Manual: TRNFLOW A Module of an Air Flow Network for Coupled Simulation with TYPE 56 (Multi Zone Building of TRNSYS)*; Solar Energy Laboratory, Univ. of Wisconsin-Madison: Madison, WI, USA, 2006.
43. Solar Energy Laboratory, Univ. of Wisconsin-Madison; TRANSSOLAR Energietechnik GmbH; CSTB—Centre Scientifique et Technique de Bâtiment; TESS—Thermal Energy System Specialists, LLC. *TRNSYS Manual: Volume 6 Multizone Building Modeling with Type56 and TRNBuild*; Solar Energy Laboratory, Univ. of Wisconsin-Madison: Madison, WI, USA, 2007; pp. 142–150.
44. Woods, J.; Winkler, J.; Christensen, D. Evaluation of the Effective Moisture Penetration Depth Model for Estimating Moisture Buffering in Buildings, Technical Report of National Renewable Energy Lab. (NREL), 2013. Available online: <http://www.osti.gov/scitech/biblio/1219896-evaluation-effective-moisture-penetration-depth-model-estimating-moisture-buffering-buildings> (accessed on 21 January 2016).
45. Yoshino, H.; Mitamura, T.; Hasegawa, K. Moisture buffering and effect of ventilation rate and volume rate of hygrothermal materials in a single room under steady state exterior conditions. *Build. Environ.* **2009**, *44*, 1418–1425. [[CrossRef](#)]
46. Catalina, T.; Woloszyn, M.; Virgone, J. Impact of Moisture Buffering on Energy Performance of Cooling Ceilings. In Proceedings of the Annex 41 International Conference, Lyon, France, 25–27 October 2006.
47. Abadie, M.; Deblois, J.P.; Mendes, N. A Comparison Exercise for Calculating Heat and Moisture Transfers Using TRNSYS and PowerDomus. Available online: <http://www.kuleuven.be/bwf/projects/annex41/protected/data/PUCPR%20Oct%202005%20Paper%20A41-T1-Br-05-2.pdf> (accessed on 6 January 2016).

48. Japan Image and Information Management Association (JIIMA), Suggested the Policy of Promoting Green Office to the Minister of Public Management. Available online: http://www.jiima.or.jp/pdf/policy_recommendations1.pdf (accessed on 12 December 2015).
49. Japanese Standards Association. *Japanese Industrial Standard Committee, JIS A 1475 Method of Test for Hygroscopic Sorption Properties of Building Materials*; Japanese Standards Association: Mita, Minato-ku, Tokyo, Japan, 2004.



© 2016 by the authors; licensee MDPI, Basel, Switzerland. This article is an open access article distributed under the terms and conditions of the Creative Commons Attribution (CC-BY) license (<http://creativecommons.org/licenses/by/4.0/>).